Joint Angle and Delay Estimation for DS-CDMA Communication Systems with Application to Reduced Dimension Space-Time 2D Rake Receivers [1]

Yung-Fang Chen and Michael D. Zoltowski

yungfang@ecn.purdue.edu   mikedz@ecn.purdue.edu
phone 765-494-9621   phone: 765-494-3512, fax: 765-494-0880
School of Electrical and Computer Engineering, Purdue University
1285 Electrical Engineering Building, West Lafayette, IN 47907-1285 U.S.A.

Submitted to the IEEE Transactions on Signal Processing

Abstract

In this paper, we propose an algorithm for the joint estimation of the angle of arrival (AOA) and delay of each dominant multipath for the desired user for use in a reduced dimension space-time RAKE receiver for DS-CDMA communications that is "near-far" resistant. After we estimate the desired spatio-frequency signal vector, we propose the 2D unitary ESPRIT algorithm as our estimator which provides closed-form as well as automatically paired AOA-delay estimates. We effectively have a single snapshot of 2D data and thus require 2D smoothing for extracting multiple snapshots. The comparative performance of two 2D smoothing schemes, pre-eigenanalysis and post-eigenanalysis 2D smoothing, is discussed. The space-time data model for the IS-95 uplink is presented. The simulation results are compared with the Cramer-Rao Bound (CRB) of the joint estimation algorithm for the space-time data model at the post-correlation processing stage. The performance of a reduced dimension space-time RAKE receiver for the IS-95 uplink using the AOA-delay estimates is assessed through Monte-Carlo simulations.

[1] This research work was supported by AFOSR under contract no. F49620-97-1-0275 and the National Science Foundation under grant no. MIPS-9708309.

1 Introduction

In this paper, we present joint angle and delay estimation algorithms [2] for both classical DS-CDMA communication systems and the IS-95 uplink, assuming known spreading waveform of the desired user and approximate bit synchronization. Our algorithm can accurately estimate the angle of arrival (AOA) and time delay for each multipath component of the desired user even under "near-far" conditions. We propose the 2D Unitary ESPRIT algorithm [2] as our estimator which provides closed-form and automatically paired 2D parameter estimates.

The joint angle and delay estimation algorithm using the shift-invariance techniques applied to the estimated channel impulse response in [3] was proposed for a single source in a multipath scenario. A joint estimation algorithm for cellular TDMA based communication systems was proposed in [4]. A angle-only estimation algorithm for DS-CDMA systems was proposed in [5], and the power control was assumed for this scheme. A propagation delay estimation algorithm in a asynchronous DS-CDMA system was proposed in [6] by using MUSIC algorithm. This algorithm was shown to combat over "near-far" problem. However, this approach needs exhaustive search and does not provide a close-form solution.

A major benefit of the joint estimation algorithm is that the number of multipaths can be larger than the number of antennas, which overcomes the limitation of separable estimation. We also present the utility of the joint angle-delay estimates in a reduced dimension space-time RAKE receiver. The AOA information is also useful for "smart" FDD downlink beamforming or geolocation problems.

The structure of this paper is as follows. Section 2 provides the space-time data models for the classical DS-CDMA communication systems and the IS-95 uplink. Section 3 gives the overview of the 2D Unitary ESPRIT algorithm. The developments of the proposed joint delay-angle estimation algorithms with two different processing orders in 2D smoothing scheme are described in Section 4. The Cramer-Rao Bound of the estimation algorithms at the post-correlation processing stage is derived in Section 5. In Section 6, we address the application of the angle and delay estimates to a reduced dimension space-time RAKE receiver for the DS-CDMA communication systems. Various Simulation results are presented in Section 7. Finally, we make conclusions in Section 8.

[2] Portions of this work were previously reported at a conference [1]

2 Space-Time Data Model

2.1 Classical DS-CDMA space-time data model

The $M \times 1$ array snapshot vector $\mathbf{x}(t)$ containing the outputs of each of the M antennas comprising the array at time t is modeled as

$$\mathbf{x}(t) = \sum_{k=1}^{P} \rho_k \sum_{m=0}^{N_b-1} \mathbf{a}(\theta_k^d) D(m) c(t - mT_b - \tau_k) + \sum_{i=1}^{J} \sum_{m=0}^{N_b-1} \mathbf{a}(\theta_i) \sigma_i D_i(m) c_i(t - mT_b) + \mathbf{n}_w(t) \tag{1}$$

where d denotes the desired user. $\mathbf{a}(\theta)$ is the spatial response of the array. For the sake of notational simplicity, we here assume that the spatial response vector depends on a single directional parameter, θ, the direction of arrival (DOA) of a given source. $1/T_b$ is the symbol rate common to all sources. P is the number of different paths the Signal of Interest (SOI) arrives from, θ_k^d denotes the directions associated with the k-th path, and τ_k is the corresponding relative delay of the k-th path. ρ_k is the complex amplitude of the k-th multipath arrival for the SOI at the reference element. $D(m)$ and $D_i(m)$ are the digital information sequences for the SOI and MUAI sources, respectively. J broadband interferers (MUAI) impinge upon the array. σ_i is the complex amplitude of the i-th interferer at the reference element of the array. $c(t)$ and $c_i(t)$ are the spreading waveforms for the SOI and i-th MUAI, respectively. The vector $\mathbf{n}_w(t)$ contains white noise. N_b is the number of bits over which all parameters characterizing the model in (1) are assumed to be constant. N_b might be quite small in cases of rapidly evolving dynamics. The spreading waveform for the i-th MUAI is modeled as

$$c_i(t) = \sum_{l=0}^{N_c-1} s_i(l) p_c(t - lT_c) \tag{2}$$

where $\frac{1}{T_c}$ is the chip rate, $s_i(l)$ is a PN sequence, $p_c(t)$ is the chip waveform assumed common to all sources, N_c is the number of chips per bit common to all MUAI's. The spreading waveform for the desired source, $c(t)$, is defined similarly but with a different PN sequence. [3]

2.2 Space-Time Data Model for IS-95 Uplink

The transmitter block diagram for the uplink of IS-95 is shown in Figure 1. Two information bits are mapped to six bits via a rate 1/3 convolutional encoder. These six bits are grouped together as an index to select one of 64 Walsh-Hadamard functions, which is then subsequently multiplied by a (time-varying) user's spreading waveform $c_i(t)$ with four chips per "Walsh" chip. Note that the period of $c_i(t)$ is 2^{42} -1. The data is further spread by two short codes $a^I(t)$ and $a^Q(t)$ with period equal to 2^{15} to create the I and Q channels, respectively. The resulting I and Q channels, which carry the

[3] Note that this model is easily modified for the case where the spreading waveform varies from bit to bit as will be seen in the the IS-95 uplink space-time data model.

same information bits, are then input to an offset-QPSK modulator with the PN modulated Q channel signal delayed by a half chip period, $T_c/2$, relative to the PN modulated I channel. The j-th symbol transmitted by the i-th user is described as

$$\mathbf{s}_i(t) = \sqrt{\mathcal{P}_i} W_i^j(t) a_i^{\mathbf{I}}(t) cos(\omega_c t) + \sqrt{\mathcal{P}_i} W_i^j(t - \frac{T_c}{2}) a_i^{\mathbf{Q}}(t - \frac{T_c}{2}) sin(\omega_c t) \ \ , \ \ 0 \leq t \leq T_w \tag{3}$$

The various quantities in (3) are described below. Define $W_i^j(t)$ as Walsh symbol, and j is referred to as the Walsh function index: $j = 1, 2, .., 64$. $\mathcal{P}_i$ is the transmitted power per symbol. ω_c is the carrier frequency in radians. T_w is the duration of a Walsh symbol. $a_i^I(t)$ and $a_i^Q(t)$ are the PN spreading codes applied to the I and Q channels, respectively:

$$a_i^I(t) = c_i(t) a^I(t) \qquad a_i^Q(t) = c_i(t) a^Q(t)$$

Denoting the chip waveform as $p(t)$,

$$\begin{aligned} a_i^I(t) &= \sum_{n=-\infty}^{\infty} a_{i,n}^I p(t - nT_c) \\ a_i^Q(t) &= \sum_{n=-\infty}^{\infty} a_{i,n}^Q p(t - nT_c), \end{aligned} \tag{4}$$

where $a_{i,n}^I$ and $a_{i,n}^Q$ are distinct PN sequences.

Similarly, for the IS-95 uplink, the baseband representation of the $M \times 1$ array snapshot vector $\mathbf{x}(t)$ containing the outputs of each of the M antennas comprising the array at time t is modeled as

$$\begin{aligned} \mathbf{x}(t) = \sum_{k=1}^{P_d} \rho_k^d \mathbf{a}(\theta_k^d)[W_d^j(t - \tau_k^d) a_d^{\mathbf{I}}(t - \tau_k^d) + jW_d^j(t - \frac{T_c}{2} - \tau_k^d) a_d^{\mathbf{Q}}(t - \frac{T_c}{2} - \tau_k^d)] + \\ \sum_{i=1}^{J} \sum_{k=1}^{P_i} \rho_k^i \mathbf{a}(\theta_k^i)[W_i^j(t - \tau_k^i) a_i^{\mathbf{I}}(t - \tau_k^i) + jW_i^j(t - \frac{T_c}{2} - \tau_k^i) a_i^{\mathbf{Q}}(t - \frac{T_c}{2} - \tau_k^i)] + \mathbf{n}_w(t) \end{aligned} \tag{5}$$

For a given user i(d denotes the desired user): P_i is the number of different paths the i-th signal arrives from, θ_k^i denotes the arrival direction of the k-th multipath, and τ_k^i is the corresponding relative delay of the k-th multipath. ρ_k^i is the complex amplitude of the k-th multipath arrival for the i-th signal at the reference element. J multi-user access interferers (MUAI) impinge upon the array. The vector $\mathbf{n}_w(t)$ represents the contribution of additive white noise.

3 Overview of 2D Unitary ESPRIT

The core of the joint angles of arrival and time delays estimation algorithms in the paper is the utilization of 2D Unitary ESPRIT which does not need time-consuming 2D exhaustive search as in the MUSIC-type algorithms. We here present a brief development of 2D Unitary ESPRIT which provides the automatically paired source azimuth and elevation angle estimates in closed-form with uniform rectangular array (URA) of $M \times L$ elements. In the final stage of the algorithm, the real and imaginary parts of the i-th eigenvalue of a matrix are one-to-one related to the respective direction cosines of the ith source relative to the two major array axes. Note that 2D Unitary ESPRIT is applicable for the problems which can be reduced to a matrix with shift-invariant property in both axes. Hence, it can be employed in a variety of applications other than 2D angle estimation including 2D harmonic retrieval problems. 2D Unitary ESPRIT offers a number of advantages. Here, we point out some of them which are related to our joint estimation problem. First, except for the final eigenvalue decomposition of dimension equal to the number of sources, it is efficiently formulated in terms of real-valued computation throughout. Second, it easily handles sources having one member of the spatial frequency coordinate pair in common.

For developing the idea of 2D Unitary ESPRIT, we describe the relations of 1-D case first. Employing the center of the uniform linear array (ULA) as the phase reference, the array manifold is conjugate centrosymmetry. For example, if the number of elements comprising the ULA M is odd, there is a sensor located at the array center and the array manifold is

$$\mathbf{a}_M(\mu) = [e^{-j(\frac{M-1}{2})\mu}, \cdots, e^{-j\mu}, 1, e^{j\mu}, \cdots, e^{j(\frac{M-1}{2})\mu}]^T \tag{6}$$

where $\mu = 2\frac{\pi}{\lambda}\Delta_x u$ with λ equal to the wavelength, Δ_x is equal to the interelement spacing, and $u = cos(\theta)$ is equal to the direction cosine relative to the array axis.

Define

$$\mathbf{Q}_M = \begin{cases} \frac{1}{\sqrt{2}} \begin{bmatrix} \mathbf{I}_K & j\mathbf{I}_K \\ \mathbf{\Pi}_K & -j\mathbf{\Pi}_K \end{bmatrix} & ; \quad \text{if } M = 2K \\ \frac{1}{\sqrt{2}} \begin{bmatrix} \mathbf{I}_K & \mathbf{0} & j\mathbf{I}_K \\ \mathbf{0}^T & \sqrt{2} & \mathbf{0}^T \\ \mathbf{\Pi}_K & \mathbf{0} & -j\mathbf{\Pi}_K \end{bmatrix} & ; \quad \text{if } M = 2K+1 \end{cases}$$

where

$$\mathbf{\Pi}_K = \begin{bmatrix} 0 & 0 & \cdots & 0 & 1 \\ 0 & 0 & \cdots & 1 & 0 \\ \vdots & \vdots & \ddots & \vdots & \vdots \\ 0 & 1 & \cdots & 0 & 0 \\ 1 & 0 & \cdots & 0 & 0 \end{bmatrix} \in \mathbf{R}^{K \times K}$$

Then, we have the real-valued manifold $\mathbf{d}_M(\mu)$:

$$\begin{aligned} \mathbf{d}_M(\mu) &= \mathbf{Q}_M^H \mathbf{a}_M(\mu) \qquad (7) \\ &= \sqrt{2} \times \left[\cos(\frac{M-1}{2}\mu), \cdots, \cos\mu, \frac{1}{\sqrt{2}}, -\sin(\frac{M-1}{2}\mu), \cdots, -\sin\mu\right]^T \end{aligned}$$

Define:

$$\mathbf{K}_1 = Re(\mathbf{Q}_{M-1}^H \mathbf{J} Q_M) \;\; ; \;\; \mathbf{K}_2 = Im(\mathbf{Q}_{M-1}^H \mathbf{J} Q_M) \tag{8}$$

where

$$\mathbf{J} = \begin{bmatrix} 0 & 1 & 0 & \cdots & 0 \\ 0 & 0 & 1 & \cdots & 0 \\ \vdots & \vdots & \vdots & \ddots & \vdots \\ 0 & 0 & 0 & \cdots & 1 \end{bmatrix} \in \mathbf{R}^{(M-1)\times M}$$

Invoking the definition of the tangent function yields the following invariance relationship satisfied by $\mathbf{d}_M(\mu)$ involving only real-valued quantities:

$$\tan\left(\frac{\mu}{2}\right)\mathbf{K}_1\mathbf{d}_M(\mu) = \mathbf{K}_2\mathbf{d}_M(\mu) \tag{9}$$

For $P < M$ sources, we define $M \times P$ real-valued AOA matrix as

$$\mathbf{D} = [\mathbf{d}_M(\mu_1), \mathbf{d}_M(\mu_2), \cdots, \mathbf{d}_M(\mu_P)]\,.$$

The real-valued manifold relation in (8) translates into the real-valued AOA matrix relation

$$\mathbf{K}_1\mathbf{D}\boldsymbol{\Omega}_\mu = \mathbf{K}_2\mathbf{D} \tag{10}$$

where $\Omega_\mu = diag\{\tan(\frac{\mu_1}{2}), \cdots, \tan(\frac{\mu_P}{2})\}$.

if $\mathbf{X}$ denotes the $M \times P$ element space data matrix containing P snapshots as columns, the signal eigenvectors may be computed as the "largest" left singular vectors of the real-valued matrix $[Re\{\mathbf{Y}\}, Im\{\mathbf{Y}\}]$, where $\mathbf{Y} = \mathbf{Q}_M^H\mathbf{X}$. Asymptotically, the $M \times P$ real-valued matrix of signal eigenvectors $\mathbf{E}_s$ is related to the real-valued $M \times P$ AOA matrix $\mathbf{D}$ as

$$\mathbf{E}_S = \mathbf{D}\mathbf{T} \tag{11}$$

where $\mathbf{T}$ is an unknown $P \times P$ real-valued matrix. Substituting $\mathbf{D} = \mathbf{E}_S\mathbf{T}^{-1}$ into (10) yields

$$\mathbf{K}_1\mathbf{E}_S\boldsymbol{\Psi} = \mathbf{K}_2\mathbf{E}_S \tag{12}$$

where $\boldsymbol{\Psi} = \mathbf{T}^{-1}\boldsymbol{\Omega}_\mu\mathbf{T}$. Thus, the eigenvalues of the $P \times P$ solution $\boldsymbol{\Psi}$ to the $(M-1) \times P$ matrix equation above are $\tan(\frac{\mu_i}{2}), i = 1, \cdots, P$.

For the 2D case, let URA of $M \times L$ elements lying in the $x - y$ plane and equi-spaced by Δ_x in the x direction and Δ_y in the y direction. In addition to $\mu = \frac{2\pi}{\lambda}\Delta_x u$, where u is the direction cosine variable relative to the $x-$ axis, we define the spatial frequency variable $\nu = \frac{2\pi}{\lambda}\Delta_y v$, where v is the direction cosine variable relative to the $y-$axis. In matrix form, the array manifold may be expressed as

$$\mathbf{A}(\mu, \nu) = \mathbf{a}_M(\mu)\mathbf{a}_L^T(\nu) \tag{13}$$

where $\mathbf{a}_L(\nu)$ is defined by (6) with M replaced by L and μ replaced by ν. Similar to the 1-D case, premultipling $A(\mu,\nu)$ by $\mathbf{Q}_M^H$ and post-multiplying by $\mathbf{Q}_L^*$, creates the $M \times L$ real-valued manifold

$$\begin{aligned}\mathbf{D}(\mu,\nu) &= \mathbf{Q}_M^H A(\mu,\nu)\mathbf{Q}_L^* \\ &= \mathbf{Q}_M^H \mathbf{a}_M(\mu)\mathbf{a}_L^T(\nu)\mathbf{Q}_L^* \\ &= \mathbf{d}_M(\mu)\mathbf{d}_L^T(\nu) \end{aligned} \quad (14)$$

Given $\mathbf{d}_M(\mu)$ satisfies the invariance relationship in (8), it follows that $\mathbf{D}(\mu,\nu)$ satisfies

$$\tan(\frac{\mu}{2})\mathbf{K}_1\mathbf{D}(\mu,\nu) = \mathbf{K}_2\mathbf{D}(\mu,\nu) \quad (15)$$

It follows that the $ML \times 1$ real-valued manifold in vector form $\mathbf{d}(\mu,\nu) = vec(\mathbf{D}(\mu,\nu))$ satisfies

$$\tan(\frac{\mu}{2})\mathbf{K}_{\mu_1}\mathbf{d}(\mu,\nu) = \mathbf{K}_{\mu_2}\mathbf{d}(\mu,\nu) \quad (16)$$

where $\mathbf{K}_{\mu_1}$ and $\mathbf{K}_{\mu_2}$ are the $(M-1)L \times ML$ matrices

$$\mathbf{K}_{\mu_1} = \mathbf{I}_L \otimes \mathbf{K}_1 \;\; ; \;\; \mathbf{K}_{\mu_2} = \mathbf{I}_L \otimes \mathbf{K}_2 \quad (17)$$

Similarly, the 1-D real-valued manifold $\mathbf{d}_L(\nu)$ satisfies $\tan(\frac{\nu}{2})\mathbf{K}_3\mathbf{d}_L(\nu) = \mathbf{K}_4\mathbf{d}_L(\nu)$, where $\mathbf{K}_3 = Re(\mathbf{Q}_{L-1}^H\mathbf{J}_2\mathbf{Q}_L), \mathbf{K}_4 = Im(\mathbf{Q}_{L-1}^H\mathbf{J}_2\mathbf{Q}_L)$. it follows that

$$\tan(\frac{\nu}{2})\mathbf{K}_{\nu_1}\mathbf{d}(\mu,\nu) = \mathbf{K}_{\nu_2}\mathbf{d}(\mu,\nu) \quad (18)$$

where $\mathbf{K}_{\nu_1}$ and $\mathbf{K}_{\nu_2}$ are the $M(L-1) \times ML$ matrices

$$\mathbf{K}_{\nu_1} = \mathbf{K}_3 \otimes \mathbf{I}_M \;\; ; \;\; \mathbf{K}_{\nu_2} = \mathbf{K}_4 \otimes \mathbf{I}_M \quad (19)$$

Consider the $ML \times P$ real-valued AOA matrix $\mathbf{D} = [\mathbf{d}(\mu_1,\nu_1),\cdots,\mathbf{d}(\mu_P,\nu_P)]$, where $\mathbf{d}(\mu,\nu) = vec(\mathbf{D}(\mu,\nu))$. (15) dictates that $\mathbf{D}$ satisfies

$$\mathbf{K}_{\mu_1}\mathbf{D}\mathbf{\Omega}_\mu = \mathbf{K}_{\mu_2}\mathbf{D} \quad (20)$$

where $\Omega_\mu = diag\{\tan(\frac{\mu_1}{2}),\cdots,\tan(\frac{\mu_P}{2})\}$. In turn, (18) dictates that $\mathbf{D}$ satisfies

$$\mathbf{K}_{\nu_1}\mathbf{D}\mathbf{\Omega}_\nu = \mathbf{K}_{\nu_2}\mathbf{D} \quad (21)$$

where $\Omega_\nu = diag\{\tan(\frac{\nu_1}{2}),\cdots,\tan(\frac{\nu_P}{2})\}$

Viewing the array output at a given snapshot as an $M \times L$ matrix, premultiply by $\mathbf{Q}_M^H$ and postmultiply by $\mathbf{Q}_L^*$, apply the $vec(\cdot)$ operator, and place the resulting $ML \times 1$ vector as a column of an $ML \times P$ data matrix $\mathbf{Y}$. Note that if $\mathbf{X}$ denotes the $ML \times P$ complex-valued element space data matrix, the relationship between $\mathbf{X}$ and $\mathbf{Y}$ may be expressed as $\mathbf{Y} = (\mathbf{Q}_L^H \otimes \mathbf{Q}_M^H)\mathbf{X}$. The approximate $ML \times P$ matrix of signal eigenvectors, $\mathbf{E}_s$, for the 2D Unitary ESPRIT is computed as the P "largest" left singular vectors of the real-valued matrix $[Re\{\mathbf{Y}\}, Im\{\mathbf{Y}\}]$. Asymptotically, $\mathbf{E}_S = \mathbf{DT}$, where $\mathbf{T}$ is an unknown $P \times P$ real-valued matrix. Substituting $\mathbf{D} = \mathbf{E}_S\mathbf{T}^{-1}$ into (20) and (21) yields the signal eigenvector relations

$$\mathbf{K}_{\mu 1}\mathbf{E}_s\mathbf{\Psi}_\mu = \mathbf{K}_{\mu 2}\mathbf{E}_s \quad where: \mathbf{\Psi}_\mu = \mathbf{T}^{-1}\mathbf{\Omega}_\mu\mathbf{T} \tag{22}$$

$$\mathbf{K}_{\nu 1}\mathbf{E}_s\mathbf{\Psi}_\nu = \mathbf{K}_{\nu 2}\mathbf{E}_s \quad where: \mathbf{\Psi}_\nu = \mathbf{T}^{-1}\mathbf{\Omega}_\nu\mathbf{T} \tag{23}$$

Automatic pairing of μ and ν spatial frequency estimates is facilitated by the fact that all of the quantities in (22) and (23) are real-valued. Thus, $\mathbf{\Psi}_\mu + j\mathbf{\Psi}_\nu$ may be spectrally decomposed as

$$\mathbf{\Psi}_\mu + j\mathbf{\Psi}_\nu = \mathbf{T}^{-1}\{\mathbf{\Omega}_\mu + j\mathbf{\Omega}_\nu\}\mathbf{T} \tag{24}$$

The 2D Unitary ESPRIT algorithm is summarized below:

1. Compute $\mathbf{E}_s$ via P "largest" left singular vectors of $[Re\{\mathbf{Y}\}, Im\{\mathbf{Y}\}]$ where $\mathbf{Y} = (\mathbf{Q}_L^H \otimes \mathbf{Q}_M^H)\mathbf{X}$ and $\mathbf{X}$ denotes the $ML \times P$ complex-valued element space data matrix.

2. (a) Compute $\mathbf{\Psi}_\mu$ as the solution to the $(M-1)L \times P$ matrix equation :
   $\mathbf{K}_{\mu 1}\mathbf{E}_s\mathbf{\Psi}_\mu = \mathbf{K}_{\mu 2}\mathbf{E}_s$.

   (b) Compute $\mathbf{\Psi}_\nu$ as the solution to the $M(L-1) \times P$ matrix equation :
   $\mathbf{K}_{\nu 1}\mathbf{E}_s\mathbf{\Psi}_\nu = \mathbf{K}_{\nu 2}\mathbf{E}_s$.

3. Compute λ_i , $i = 1, ..., P.$ as the eigenvalues of the $P \times P$ matrix $\mathbf{\Psi}_\mu + j\mathbf{\Psi}_\nu$.

4. Compute spatial frequency estimates $\mu_i = 2tan^{-1}(Re(\lambda_i)), \nu_i = 2tan^{-1}(Im(\lambda_i))$, $i = 1, ..., P$.

Note that the maximum number of sources 2D Unitary ESPRIT can handle is minimum $\{M(L-1), L(M-1)\}$, assuming that at least $\frac{P}{2}$ snapshots are available (it is inherently effecting a forward-backward average that effectively doubles the number of snapshots.). If only a single snapshot is available, one can extract $\frac{P}{2}$ or more identical rectangular subarrays out of the overall array to get the effect of multiple snapshots, thereby decreasing the maximum number of sources that can be handled.

4 Joint Angle and Delay Estimation

Our goal is to jointly estimate the AOA and relative delay parameter pairs $\{(\theta_i^d, \tau_i^d)\}, i = 1, \cdots, P$, under multipath propagation and "near-far" conditions. We consider applying the 2D Unitary ESPRIT algorithm to the data model formulated in such a way as to exhibit the shift-invariance property required by ESPRIT. The desired data model may be achieved by adapting the space-frequency 2D processing scheme previously proposed by Zoltowski [7] as shown in Figure 2. This 2D RAKE receiver was proposed for direct sequence spread spectrum communication systems and achieve two primary goals: (1) optimal combination of the desired user's multipath in a RAKE-like receiver fashion and (2) simultaneous cancellation of strong multi-user access interference and other forms of interference. To achieve these goals, it only exploits: (1) known spreading waveform of desired user, (2) approximate bit synchronization for desired user and (3) known maximum multipath time-delay spread τ_{max}.

4.1 Blind Adaptive 2D RAKE Receiver for DS-CDMA Based on Space-Frequency MVDR Processing

As shown in Figure 2 (the number of samples per chip $L_c = 2$, $\tau_{max} = 8\mu sec$, $T_b = 128\mu sec$), The received signal at each antenna is sampled at a rate L_c/T_c. The sampled output of each antenna is passed through a filter whose impulse response is an oversampled version of the time-reverse and conjugate of the spreading waveform of the desired user expressed as $h[n] = c^*[-n]$, where $c[n] = c(nT_c/L_c)$.

After passing the output of each antenna through the matched filter, one estimates the signal plus interference space-frequency correlation matrix, $\hat{\mathbf{K}}_{S+I+N}$, during that portion of the bit interval where the RAKE fingers occur, and the interference alone space-frequency correlation matrix, $\hat{\mathbf{K}}_{I+N}$, during that portion of the bit interval away from the fingers. Denote $MN_s \times 1$ post-correlation space-time snapshot $\mathbf{x}_{st}[n]$ is equal to:

$$[x_1[n], x_2[n], \cdots x_M[n], x_1[n+1], \cdots, x_1[n+(N_s-1)], \cdots x_M[n+(N_s-1)]]^T,$$

where $N_s = \lceil \frac{L_c \tau_{max}}{T_c} \rceil$ = number of samples encompassing the maximum multipath time delay spread τ_{max} and $x_j[n]$ denote the sample of the output of the j-th antenna after the matched filter.

The $ML \times ML$ signal plus interference (plus noise) space-frequency correlation matrix is estimated as

$$\hat{\mathbf{K}}_{S+I+N} = \frac{1}{N_b} \sum_{l=0}^{N_b-1} \{(\mathbf{T}_C \otimes \mathbf{I}_M)^H \mathbf{x}_{st}[lN_t]\}\{\mathbf{x}_{st}^H[lN_t](\mathbf{T}_C \otimes \mathbf{I}_M)\} \tag{25}$$

The interference (plus noise) space-frequency correlation matrix is estimated as

$$\hat{\mathbf{K}}_{I+N} = \frac{1}{N_b N_{AF}} \sum_{l=0}^{N_b-1} \sum_{n=1}^{N_{AF}} \{(\mathbf{T}_C \otimes \mathbf{I}_M)^H \mathbf{x}_{st}[nL_s + lN_t + N_s]\}\{\mathbf{x}_{st}^H[nL_s + lN_t + N_s](\mathbf{T}_C \otimes \mathbf{I}_M)\} \tag{26}$$

where $N_t = N_c L_c$ = total number of samples in one bit period, L_s is the number of sample points which the length N_s window is slid over in forming the new space-time snapshot after averaging in the current space-time snapshot, and $N_{AF} \leq \lfloor \frac{N_t - 2N_s}{L_s} \rfloor$ is the number of the snapshot extracted away from the "RAKE fingers". $\mathbf{T}_C^H$ is simply the L columns of the N_s pt. DFT matrix for computing the L spectrum values around DC component. $\otimes$ denotes the *Kronecker* product. [4]

The optimum weight vector $\hat{\mathbf{w}}_{opt}$ for combining the L spectrum values computed from the N_s pt. DFT of a time window with N_s time samples encompassing the "fingers" at each of the M antennas is the "largest" generalized eigenvector of the $ML \times ML$ space-frequency matrix pencil $\{\hat{\mathbf{K}}_{S+I+N}, \hat{\mathbf{K}}_{I+N}\}$, which is the solution to the SINR maximizing criterion:

$$\underset{\mathbf{w}}{\text{Maximize}} \quad \frac{\mathbf{w}^H \mathbf{K}_{S+I+N} \mathbf{w}}{\mathbf{w}^H \mathbf{K}_{I+N} \mathbf{w}}$$

For the 64-ary orthogonal modulation used in the IS-95 uplink, we need to contruct 64 matched filters forming a filter bank at each antenna receiver. Therefore, this matrix pencil is estimated from the aforementioned matched filter outputs containing the "fingers" in a decision directed fashion [8, 9].

4.2 Joint Angle and Delay Estimation Algorithms

For the space-time data model of the classical DS-CDMA communication systems, the asymptotic structure of $\hat{\mathbf{K}}_{S+I+N}$ may be expressed as:

$$\mathbf{K}_{S+I+N} = \sigma_s^2 (\sum_{i=1}^{P} g_i \mathbf{f}(\tau_i) \otimes \mathbf{a}(\theta_i))(\sum_{i=1}^{P} g_i \mathbf{f}(\tau_i) \otimes \mathbf{a}(\theta_i))^H + \mathbf{K}_{I+N} \tag{27}$$

where $\sigma_b^2 = E[D^2(n)]$ and we have dropped superscript d for notational simplicity. Assuming the antenna elements to be equi-spaced along a line and well-calibrated, g_i is the complex gain of the i-th multipath arrival, τ_i is the relative time-delay of the i-th multipath arrival, and $\mathbf{a}(\theta_i)$ is the array manifold $= [1, e^{j\mu}, \cdots, e^{j(M-1)\mu}]^T$, where $\mu = \frac{2\pi}{\lambda} \Delta_x \sin\theta_i$ with λ is the wavelength, Δ_x is the interelement spacing, and θ_i is the angle of arrival relative to the normal to the array axis. $\mathbf{f}(\tau_i) = \mathbf{v}(\tau_i) \odot \mathbf{s}$ where $\odot$ is the Schur product and

$$\mathbf{s} = [S(-K\Delta f), ..., S(-\Delta f), S(0), S(\Delta f), ..., S(K\Delta f)]^T, \tag{28}$$

where L=2K+1 and $S(f)$ is $sinc^2(fT_c)$ in the case of a rectangular chip waveform, for example. $\frac{1}{T_c}$ is the chip rate, $\mathbf{v}(\tau_i) = e^{-jK\nu}[1, e^{j\nu}, \cdots, e^{j2K\nu}]^T$, where $\nu = 2\pi\Delta f \tau_i$. Typically, $\Delta f = \frac{1}{\tau_{max}}$.

[4] The *Kronecker* product $\otimes$ of a $p \times q$ matrix $\mathbf{A}$ and an $m \times n$ matrix $\mathbf{B}$ is the $pm \times qn$ matrix defined by

$$\mathbf{A} \otimes \mathbf{B} = \begin{bmatrix} a_{11}\mathbf{B} & a_{12}\mathbf{B} & \cdots & a_{1q}\mathbf{B} \\ a_{21}\mathbf{B} & a_{22}\mathbf{B} & \cdots & a_{2q}\mathbf{B} \\ \vdots & & & \vdots \\ a_{p1}\mathbf{B} & a_{p2}\mathbf{B} & \cdots & a_{pq}\mathbf{B} \end{bmatrix}$$

The "largest" generalized eigenvector of the asymptotic $ML \times ML$ matrix pencil $\{\mathbf{K}_{S+I+N}, \mathbf{K}_{I+N}\}$ is

$$\mathbf{w}_{opt} = \mathbf{K}_{I+N}^{-1}\mathbf{e}_s, \tag{29}$$

where the post-correlation space-frequency signature of the desired user

$$\mathbf{e}_s = \sigma_s \sum_{i=1}^{P} g_i \mathbf{f}(\tau_i) \otimes \mathbf{a}(\theta_i) \tag{30}$$

Thus, $\mathbf{e}_s = \mathbf{K}_I \mathbf{w}_{opt}$ and the $ML \times 1$ estimated signal vector

$$\hat{\mathbf{e}}_s = \hat{\mathbf{K}}_I \hat{\mathbf{w}}_{opt} \approx \sigma_s \sum_{i=1}^{P} g_i \mathbf{f}(\tau_i) \otimes \mathbf{a}(\theta_i) \tag{31}$$

De-stacking the $M \times 1$ sub-vectors of $\hat{\mathbf{e}}_s$ through the $mat(\cdot)$ operator yields the $M \times L$ matrix:

$$\hat{\mathbf{E}}_s = mat(\hat{\mathbf{e}}_s) = mat(\hat{\mathbf{K}}_I \hat{\mathbf{w}}_{opt}) \approx \sigma_s \sum_{i=1}^{P} g_i \mathbf{a}(\theta_i) \mathbf{f}^T(\tau_i) \tag{32}$$

We consider applying 2D Unitary ESPRIT to $\hat{\mathbf{E}}_s$ so that the final step yields eigenvalues of the form $\tan\{\frac{\mu_i}{2}\} + j\tan\{\frac{\nu_i}{2}\}$, where $\mu_i = \frac{2\pi}{\lambda}\Delta_x \sin\theta_i$ and $\nu_i = 2\pi\frac{\tau_i}{\tau_{max}}, i = 1.\cdots, P$. Before we can apply the 2D Unitary ESPRIT algorithm, we need to adjust the structure of $\hat{\mathbf{E}}_s$ such that the matrix exhibits the shift-invariance property along both the space and frequency dimensions. Since we know the spectrum of the chip waveform, we may divide out the "amplitude taper" represented by $\mathbf{s}$ in $\mathbf{f}(\tau_i) = \mathbf{v}(\tau_i) \odot \mathbf{s}$. To this end, define $\mathbf{\Gamma} = diag(\mathbf{s})$. Post-multiplying $\hat{\mathbf{E}}_s$ by $\mathbf{\Gamma}^{-1}$ yields

$$\hat{\mathbf{E}}_s^{'} \approx \sigma_s \sum_{i=1}^{P} g_i \mathbf{a}(\theta_i) \mathbf{v}^T(\tau_i) \tag{33}$$

However, we effectively have a single snapshot of 2D data and thus require 2D smoothing for extracting multiple snapshots. Note that the factor $e^{-jK\nu}$ in $\mathbf{v}(\tau_i)$ can be absorbed in g_i such that $\mathbf{a}(\theta_i)$ and $\mathbf{v}(\tau_i)$ both have Vandermonde structure which allows us to perform 2D smoothing. We propose two different orders of processing, pre-eigenanalysis 2D smoothing and post-eigenanalysis 2D smoothing, prior to applying 2D Unitary ESPRIT. These schemes are discussed below.

4.2.1 Post-eigenanalysis 2D smoothing

As pointed out before, we need at least $P/2$ snapshots to handle P multipaths. Since there is effectively a single snapshot available after computing $\hat{\mathbf{e}}_s$, we can apply a 2D smoothing technique to $\hat{\mathbf{E}}_s^{'}$ to extract $P/2$ or more identical rectangular subarrays out of the overall pseudo-array to get the effect of multiple snapshots (refer to Figure 3). Note that the maximum number of sources 2D Unitary ESPRIT can handle is minimum $\{(m_1-1)m_2, m_1(m_2-1)\}$, given that the size of the subarray is $m_1 \times m_2$ and the number of extracted snapshots is $(M-m_1+1)\times(L-m_2+1)$. Therefore, these relationships must be satisfied:

$$min\{(m_1-1)m_2, m_1(m_2-1)\} \leq P \;\; and \;\; (M-m_1+1)\times(L-m_2+1) \geq \frac{P}{2} \tag{34}$$

Let $\mathbf{E}^{(m,l)}, 1 \leq m \leq (M-m_1+1), 1 \leq l \leq (L-m_2+1)$ denote the (m,l)-th extracted snapshot with dimension $m_1 \times m_2$. Applying the $vec(\cdot)$ operator, we stack the columns of $\mathbf{E}^{(m,l)}$ to form the $m_1m_2 \times 1$ vector $\mathbf{e}^{(m,l)}$. We then form an $m_1m_2 \times (M-m_1+1)(L-m_2+1)$ matrix $\mathbf{X} = [\mathbf{e}^{(1,1)}, \mathbf{e}^{(2,1)}, \cdots, \mathbf{e}^{(M-m_1+1,L-m_2+1)}]$ which plays the role of the data matrix needed for 2D Unitary ESPRIT. The subsequent steps of the 2D Unitary ESPRIT algorithm are easily applied to calculate $\{(\theta_i, \tau_i)\}, i = 1, \cdots, P$.

Summary of the joint estimation algorithm with post-eigenanalysis 2D smoothing

1. Compute $\mathbf{w}_{opt}$ as the "largest" generalized eigenvector of space-frequency matrix pencil $\{\hat{\mathbf{K}}_{S+I+N}, \hat{\mathbf{K}}_{I+N}\}$, and estimate $ML \times 1$ signal vector $\mathbf{e}_s$ by: $\hat{\mathbf{e}}_s = \hat{\mathbf{K}}_{I+N}\mathbf{w}_{opt}$.

2. De-stacking the $ML \times 1$ sub-vectors of $\hat{\mathbf{e}}_s$ through the matrix operator $mat(\cdot)$ yields the $M \times L$ matrix $\mathbf{E} = mat\{\hat{\mathbf{e}_s}\}$. Then, applying 2D smootihing technique to $\mathbf{E}\mathbf{\Gamma}^{-1}$ to get $\mathbf{E}^{(i,j)}$ with the sub-matrix size equal to $m_1 \times m_2$, and arranging $\{\mathbf{E}^{(i,j)}, 1 \leq i \leq M-m_1+1; 1 \leq j \leq L-m_2+1\}$ as $\mathbf{X} = \left[\mathbf{e}^{(1,1)}, \mathbf{e}^{(2,1)}, \cdots, \mathbf{e}^{(M-m_1+1,L-m_2+1)}\right]$, $\mathbf{e}^{(i,j)} = vec(\mathbf{E}^{(i,j)})$.

3. Compute $\mathbf{E}_s^{'}$ via the P "largest" left singular vectors of $[Re(\mathbf{Y}), Im(\mathbf{Y})]$ which are associated with the first P largest singular value over some preset threshold, where $\mathbf{Y} = (\mathbf{Q}_{m_2}^H \otimes \mathbf{Q}_{m_1}^H)\mathbf{X}$.

4. (a) Compute $\mathbf{\Psi}_\mu$ as the solution to the $(m_1-1)m_2 \times P$ matrix equation $\mathbf{K}_{\mu1}\mathbf{E}_s^{'}\mathbf{\Psi}_\mu = \mathbf{K}_{\mu2}\mathbf{E}_s^{'}$.

   (b) Compute $\mathbf{\Psi}_\nu$ as the solution to the $m_1(m_2-1) \times P$ matrix equation $\mathbf{K}_{\nu1}\mathbf{E}_s^{'}\mathbf{\Psi}_\nu = \mathbf{K}_{\nu2}\mathbf{E}_s^{'}$.

5. Compute λ_i, $i = 1, ..., P$. as the eigenvalues of the $P \times P$ matrix $\mathbf{\Psi}_\mu + j\mathbf{\Psi}_\nu$.

6. Compute the spatial frequency estimates :
   $\mu_i = 2\arctan(Re(\lambda_i))$, $\nu_i = \arctan(Im(\lambda_i))$, $i = 1, ..., P.$, then map the spatial frequency μ_i and ν_i to the AOA and multipath time delay by $\theta_i = 180\arcsin(\frac{\mu}{\pi})/\pi$ (in degree) and $\tau_i = (\frac{T_c}{L_c})N_s\nu_i/(2\pi)$.

4.2.2 Pre-eigenanalysis 2D smoothing

As an alternative, we may effect 2D smoothing on each original space-frequency snapshot vector to generate multiple snapshots with lower dimension $m_1 \times m_2$ and form the smoothed version of the correlation matrix pencil denoted $\{\overline{\mathbf{K}}_{S+I+N}, \overline{\mathbf{K}}_{I+N}\}$. Note that we need to post-multiply each space-frequency snapshot by $\mathbf{\Gamma}^{-1}$ to achieve the required Vandermonde structure before performing 2D smoothing (This also facilitates the use of forward-backward averaging). The effect of 2D smoothing is to "decorrelate" the multipaths such that we can choose the P $m_1 m_2 \times 1$ generalized "largest" eigenvectors of the smoothed version of $\{\mathbf{K}_{S+I+N}, \mathbf{K}_{I+N}\}$ as the P "snapshots". Denote $\mathbf{E} = [\mathbf{e}_1 \vdots \mathbf{e}_2 \vdots \cdots \vdots \mathbf{e}_P]$, where $\mathbf{e}_i$ is the i-th "largest" generalized eigenvector of $\{\overline{\mathbf{K}}_{S+I+N}, \overline{\mathbf{K}}_{I+N}\}$. The subspace spanned by $\overline{\mathbf{X}} = \overline{\mathbf{K}}_{I+N}\mathbf{E}$ will be the same as the subspace spanned by $\mathbf{A}^{'} = [\mathbf{a}^{'}(\theta_1, \tau_1), \cdots, \mathbf{a}^{'}(\theta_P, \tau_P)]$, where $\mathbf{a}^{'}(\theta_i, \tau_i) = \mathbf{v}^{'}(\tau_i) \otimes \mathbf{a}^{'}(\theta_i), 1 \le i \le P$; the dimensions of $\mathbf{v}^{'}(\tau_i)$ and $\mathbf{a}^{'}(\theta_i)$ are $m_2 \times 1$ and $m_1 \times 1$ respectively, which are defined similarly as $\mathbf{v}(\tau_i)$ and $\mathbf{a}(\theta_i)$. It follows that we can apply the 2D Unitary ESPRIT algorithm to the $m_1 m_2 \times P$ matrix $\overline{\mathbf{X}}$ for the joint AOA-delay estimation.

Summary of the joint estimation algorithm with pre-eigenanalysis 2D smoothing

1. Apply 2D smoothing to the snapshots of "fingers" portion and away from the "fingers" portion where the snapshots are deconvoluted by post-multiplying $\mathbf{\Gamma}^{-1}$, and form the "decorrelated" space-frequency matrix pencil $\{\hat{\overline{\mathbf{K}}}_{S+I+N}, \hat{\overline{\mathbf{K}}}_{I+N}\}$ with the dimension equal to $m_1 m_2 \times m_1 m_2$.

2. Compute the first P "largest" generalized eigenvector $\mathbf{e}_1, \cdots, \mathbf{e}_P$ which are associated with the first P "largest" generalized eigenvalues of the space-frequency matrix pencil $\{\hat{\overline{\mathbf{K}}}_{S+I+N}, \hat{\overline{\mathbf{K}}}_{I+N}\}$ over some preset threshold, and form $m_1 m_2 \times P$ matrix $\overline{\mathbf{X}} = \hat{\overline{\mathbf{K}}}_{I+N}[\mathbf{e}_1, \cdots, \mathbf{e}_P]$.

3. Compute $\mathbf{E}_s^{'}$ via the first P "largest" left singular vectors of $[Re(\mathbf{Y}), Im(\mathbf{Y})]$, where $\mathbf{Y} = (\mathbf{Q}_{m_2}^H \otimes \mathbf{Q}_{m_1}^H)\overline{\mathbf{X}}$.

4. (a) Compute $\mathbf{\Psi}_\mu$ as the solution to the $(m_1 - 1)m_2 \times P$ matrix equation $\mathbf{K}_{\mu 1}\mathbf{E}_s^{'}\mathbf{\Psi}_\mu = \mathbf{K}_{\mu 2}\mathbf{E}_s^{'}$

   (b) Compute $\mathbf{\Psi}_\nu$ as the solution. to the $m_1(m_2 - 1) \times P$ matrix equation $\mathbf{K}_{\nu 1}\mathbf{E}_s^{'}\mathbf{\Psi}_\nu = \mathbf{K}_{\nu 2}\mathbf{E}_s^{'}$.

5. Compute λ_i, $i = 1, ..., P.$ as the eigenvalues of the $P \times P$ matrix $\mathbf{\Psi}_\mu + j\mathbf{\Psi}_\nu$.

6. Compute the spatial frequency estimates :
   $\mu_i = 2tan^{-1}(Re(\lambda_i))$, $\nu_i = tan^{-1}(Im(\lambda_i))$, $i = 1, ..., P$, then map the spatial frequency μ_i and ν_i to the AOA and multipath time delay by $\theta_i = 180 \arcsin(\frac{\mu}{\pi})/\pi$ (in degree) and $\tau_i = (\frac{T_c}{L_c})N_s\nu_i/(2\pi)$.

5 Cramer-Rao Bound

The Cramer-Rao Bound (CRB) was derived in [6] for the delay estimation of the classical DS-CDMA communication system, and it showed that the CRB on an estimator of a particular ray's propagation delay - given by the appropriate diagonal element of the CRB(τ) - is independent of the mean power of the other rays, or is independent of the "near-far" problem. In this section, we will derive the CRB for the joint AOA-delay estimation algorithms applied to the IS-95 uplink signal model. Here for simplicity of analysis due to more complicated modulation scheme in the IS-95 uplink with OQPSK spread, we try to derive the CRB for the AOA and delay estimation at the post-correlation processing stage. The derivation closely follows the procedures in [4, 10]. We also assumed the output of the matched filter contributed from the interference plus noise with Gaussian process and the "correct" matched filter output branches which contain "fingers" are chosen by using an initialization algorithm, training sequence, or in the decision directed mode of operation. Then, for the n-th Walsh symbol period, we have the $MN_s \times 1$ vector:

$$\mathbf{x}_{RF}[n] = \sum_{k=1}^{P} \rho_k \mathbf{t}(\tau_k) \otimes \mathbf{a}(\theta_k) + \mathbf{n}[n] = \mathbf{d} + \mathbf{n}[n] \tag{35}$$

where $\mathbf{x}_{RF}[n]$ is the space-time snapshot containing the "fingers" corresponding to the matched filter output of the "true" transmitted Walsh symbol. $\mathbf{d}$ is the post-correlation space-time signature of the desired user that describes the gain and phase of each RAKE finger across space and time:

$$\mathbf{d} = \sum_{k=1}^{P} \rho_k \mathbf{t}(\tau_k) \otimes \mathbf{a}(\theta_k^d), \tag{36}$$

$\mathbf{t}(\tau) = \left[\begin{array}{cccc} r_{cc}\left(-\tau\right) & r_{cc}\left(\frac{T_c}{L_c}\text{-}\tau\right) & \cdots & r_{cc}\left((N_s\text{-}1)\frac{T_c}{L_c}\text{-}\tau\right) \end{array} \right]^T$, and $r_{cc}(\tau)$ is the autocorrelation function for the SOI's spreading waveform, $c(t)$. In the case where the chip waveform, $p_c(t)$, is rectangular and the processing gain is large, $r_{cc}(\tau)$ approximately has the following triangular shape:

$$r_{cc}(\tau) = \begin{cases} 1 - \frac{|\tau|}{T_c} & \text{if} \quad |t| \leq T_c \\ 0 & \text{if} \quad |t| > T_c \end{cases} \tag{37}$$

$\mathbf{n}[n]$ represents the contribution of interference and Gaussian noise after the matched filter $\sim \mathcal{N}(\mathbf{0}, \mathbf{K}_{I+N}^{st})$. For Gaussian noise only case, which will be used in a simulation setup for the simplicity of the performance comparison to the CRB, we have:

$$\mathbf{K}_{I+N}^{st} = \sigma_N^2 \cdot \mathbf{C}_N \otimes \mathbf{I}_M \tag{38}$$

where $\mathbf{C}_N$ is a Toeplitz-symmetric matrix whose first column is $r_{cc}(\frac{mT_c}{L_c}), m = 0, \cdots, N_s - 1$.

For N_w Walsh symbol durations, the density function and the log-likelihood function of the observed process in this model can be expressed as:

$$\mathbf{f}_{\boldsymbol{\alpha}}(\mathbf{x}_{RF}[1], \mathbf{x}_{RF}[2], ..., \mathbf{x}_{RF}[N_w]) =$$
$$(\pi)^{-MN_S N_w} \parallel \mathbf{K}_{I+N} \parallel^{-N_w} exp\left\{ - \sum_{n=1}^{N_w} [\mathbf{x}_{RF}[n] - \mathbf{d}]^H \mathbf{K}_{I+N}^{-1} [\mathbf{x}_{RF}[n] - \mathbf{d}] \right\} \tag{39}$$

$$\begin{aligned}\ln(f_{\boldsymbol{\alpha}}(\mathbf{x}_{RF}[1],...,\mathbf{x}_{RF}[N_w])) &= \ln(L(\boldsymbol{\alpha}))\\ &= const - N_w \ln\{\| \mathbf{K}_{I+N} \|\} \\ &- \sum_{n=1}^{N_w}[\mathbf{x}_{RF}[n]-\mathbf{d}]^H\{\mathbf{K}_{I+N}\}^{-1}[\mathbf{x}_{RF}[n]-\mathbf{d}]\end{aligned} \tag{40}$$

The parameter vector is

$$\boldsymbol{\alpha} = [\sigma_N^2, Re\{\rho_1\}, Im\{\rho_1\}, \cdots, Re\{\rho_P\}, Im\{\rho_P\}, \boldsymbol{\theta}, \boldsymbol{\tau}]$$

and the Fisher information matrix is

$$J(\boldsymbol{\alpha}) = E\left\{[\tfrac{\partial}{\partial\boldsymbol{\alpha}}\ln(L(\boldsymbol{\alpha}))][\tfrac{\partial}{\partial\boldsymbol{\alpha}}\ln(L(\boldsymbol{\alpha}))]^T\right\}$$

Relating the above model to $\hat{\mathbf{h}}(t) = \boldsymbol{\Xi}(\theta,\tau)\boldsymbol{\beta}(t) + \mathbf{e}(t)$ in [4], but substituting the color noise $\mathbf{n}(t)$ for the white noise $\mathbf{e}(t)$, we can derive the CRB for the joint estimation algorithms:

$$\mathbf{CRB}(\theta,\tau) = \frac{1}{2N_w}[Re\{\mathbf{B}^H\mathbf{D}^H(\mathbf{K}_{I+N}^{-1} - \mathbf{K}_{I+N}^{-1}\mathbf{U}(\mathbf{U}^H\mathbf{K}_{I+N}^{-1}\mathbf{U})^{-1}\mathbf{U}^H\mathbf{K}_{I+N}^{-1})\mathbf{D}\mathbf{B}\}]^{-1} \tag{41}$$

where $\mathbf{B} = \mathbf{I}_2 \otimes diag(\boldsymbol{\rho})$, $\mathbf{D} = [\mathbf{T}\diamond\mathbf{A}', \mathbf{T}'\diamond\mathbf{A}]$, and $\mathbf{U} = \mathbf{T}\diamond\mathbf{A}$; $\diamond$ is the "Khatri-Rao" product, which is a columnwise Kronecker product:$\mathbf{A}\diamond\mathbf{B} = [\mathbf{a}_1\otimes\mathbf{b}_1, \mathbf{a}_2\otimes\mathbf{b}_2\cdots]$.

$$\begin{array}{lcl}\mathbf{A} = [\mathbf{a}(\theta_1),\cdots,\mathbf{a}(\theta_P)] & ; & \mathbf{A}' = [\frac{\partial\mathbf{a}}{\partial\theta_1}(\theta_1),\cdots,\frac{\partial\mathbf{a}}{\partial\theta_P}(\theta_P)]\\ \mathbf{T} = [\mathbf{t}(\tau_1),\cdots,\mathbf{t}(\tau_P)] & ; & \mathbf{T}' = [\frac{\partial\mathbf{t}}{\partial\tau_1}(\tau_1),\cdots,\frac{\partial\mathbf{t}}{\partial\tau_P}(\tau_P)]\end{array}$$

6 Reduced Dimension Processing VIA Joint Angle-Delay Estimation

In this section, we develop the reduced dimension space-time 2D RAKE receiver related to [9] with knowledge of $\{(\theta_i,\tau_i)\}$. As substantiated in [9], reduced dimension processing offers faster convergence if the compression matrix is designed judiciously. For the given i-th AOA-delay pair (θ_i,τ_i), the optimal beamformer for the corresponding multipath arrival is given by the well-known Weiner solution $\mu_i\mathbf{R}_{I+N}^{-1}\mathbf{a}(\theta_i)$, where $\mu_i = \frac{1}{\mathbf{a}^H(\theta_i)\mathbf{R}_{I+N}^{-1}\mathbf{a}(\theta_i)}$ and $\mathbf{R}_{I+N}$ is the interference plus noise spatial correlation matrix. The approach is to optimally combine each multipath component after applying the optimal beamforming weight vector to the corresponding time sample of the multipath arrival at each antenna. The proposed reduced-dimension space-time RAKE receiver exploiting the estimates $\{(\hat{\theta}_i,\hat{\tau}_i)\}, i = 1,\cdots,P$, is as follows. We may rewrite the maximizing SINR criterion with the compression matrix $\mathbf{T}_r$ as:

$$\underset{\mathbf{w}_r}{\text{Maximize}} \quad \frac{\mathbf{w}_r^H\mathbf{K}_{S+I+N}^r\mathbf{w}_r}{\mathbf{w}_r^H\mathbf{K}_{I+N}^r\mathbf{w}_r},$$

where

$$\mathbf{K}_{S+I+N}^r = \mathbf{T}_r^H\hat{\mathbf{K}}_{S+I+N}^{st}\mathbf{T}_r \quad \mathbf{K}_{I+N}^r = \mathbf{T}_r^H\hat{\mathbf{K}}_{I+N}^{st}\mathbf{T}_r, \tag{42}$$

and $\{\hat{\mathbf{K}}_{S+I+N}^{st}, \hat{\mathbf{K}}_{I+N}^{st}\}$ is the full dimension space-time matrix pencil, which is estimated in a similar way as in Figure 2 by using time samples instead of the selected frequency samples. Similar to the expression of the estimation of the space-frequency correlation matrix pencil, the $MN_s \times MN_s$ signal plus interference (plus noise) space-time correlation matrix is estimated as

$$\hat{\mathbf{K}}_{S+I+N}^{st} = \frac{1}{N_b} \sum_{l=0}^{N_b-1} \mathbf{x}_{st}[lN_t]\mathbf{x}_{st}^H[lN_t] \tag{43}$$

The interference (plus noise) space-time correlation matrix is estimated as

$$\hat{\mathbf{K}}_{I+N}^{st} = \frac{1}{N_b N_{AF}} \sum_{l=0}^{N_b-1} \sum_{n=1}^{N_{AF}} \mathbf{x}_{st}[nL_s + lN_t + N_s]\mathbf{x}_{st}^H[nL_s + lN_t + N_s] \tag{44}$$

Making use of the estimated AOA and delay parameter pairs, we form the compression matrix $\mathbf{T}_r$ as:

$$\mathbf{T}_r = [\mu_1 \boldsymbol{\delta}_1 \otimes \hat{\mathbf{R}}_{I+N}^{-1}\mathbf{a}(\hat{\theta}_1) \vdots \cdots \vdots \mu_P \boldsymbol{\delta}_P \otimes \hat{\mathbf{R}}_{I+N}^{-1}\mathbf{a}(\hat{\theta}_P)] \tag{45}$$

where

$$\hat{\mathbf{R}}_{I+N} = \frac{1}{N_s} \sum_{l=0}^{N_s-1} \mathbf{\Gamma}_l^T \hat{\mathbf{K}}_{I+N}^{st} \mathbf{\Gamma}_l \tag{46}$$

with

$$\mathbf{\Gamma}_l = \begin{bmatrix} \mathbf{0} \\ \mathbf{I} \\ \mathbf{0} \end{bmatrix} \begin{array}{l} (l-1)M \\ M \\ (N_s - l)M \end{array}$$

and $\boldsymbol{\delta}_i = [0, \cdots, 0, 1, 0, \cdots .0]^T$, where the 1 is in the i-th position corresponding to the time sample closest to the estimate of the relative delay of the i-th multipath arrival.

We previously proposed reduced dimension space-time 2D RAKE receivers for the IS-95 uplink through a pre-spatial processing scheme followed by the beamspace-frequency processing in a decision directed fashion [8, 9]. With the paired angle and delay estimated parameters, we can calculate the decision variable for each possible Walsh symbol at a given symbol period as:

$$\|\hat{\mathbf{w}}_r^H(\mathbf{T}_r^H \mathbf{x}_{RF}^{(j)}[n])\|^2, j = 1, \cdots, 64, \tag{47}$$

where $\mathbf{x}_{RF}^{(j)}[n]$ is a space-time snapshot from the j-th matched filter encompassing the "fingers" at the n-th Walsh symbol period, and $\hat{\mathbf{w}}_r$ is the "largest" generalized eigenvector of the "compressed" $P \times P$ matrix pencil $\{\hat{\mathbf{K}}_{S+I+N}^r, \hat{\mathbf{K}}_{I+N}^r\}$, which is estimated over the pass few Walsh symbol periods.

7 Simulation Results

Illustrative simulations are presented demonstrating the efficacy of the joint angle-delay estimation algorithms for classical DS-CDMA communication systems and the IS-95 uplink signal model. The simulation results for the application to the reduced dimension space-time 2D RAKE receiver are also presented.

7.1 Simulation Results for the Classical DS-CDMA

A linear array of 8 antennas equi-spaced by a half-wavelength was employed. Both the desired source and the interferers were DS-CDMA signals with different maximal length sequences and 127 chips per bit. A rectangular chip waveform was employed. The chip rate was 1 MHz and the sampling rate was 2 MHz. The two DS-CDMA interferers arrived at 50^o and -35^o, respectively, with power levels of 15 dB and 20 dB above the desired user's direct path, respectively. A three-ray multipath model was used for the desired source wherein the direct path arrived at an angle of 0^o relative to broadside with an SNR of -5 dB per element. The SNR of the specular multipaths were 1 and 2.5 dB below that of the direct path and phase shifted by 45^o and 90^o at the first antenna element. The specular path for the SOI arrived at 8^o with delay by four and half chips, the other arrived at 15^o with delay by seven chips. The multipath delay spread was assumed to be 8 μs dictating 16 half-chip spaced taps at each of the 8 antennas.

Figure 4 displays the estimated AOA and delay "scatter plots" obtained from 256 independent runs with the space-frequency correlation matrix pencil $\{\hat{\mathbf{K}}_{S+I+N}, \hat{\mathbf{K}}_{I+N}\}$ averaged over 12 bit periods under the assumption that the channel characteristics remain approximately constant. Note that for estimating $\hat{\mathbf{K}}_{I+N}$, we extracted 70 snapshots per bit interval over that portion of away from "RAKE fingers" by sliding the 8 microsecond time window a chip per time. The space-frequency correlation matrices $\{\hat{\mathbf{K}}_{S+I+N}, \hat{\mathbf{K}}_{I+N}\}$ were 72×72 if 9 frequency samples centered at DC were retained from 16 pt. DFT. The subarray size (m_1, m_2) was chosen to be $(6, 5)$. Therefore, $\{\hat{\overline{\mathbf{K}}}_{S+I+N}, \hat{\overline{\mathbf{K}}}_{I+N}\}$ were 30×30.

It is observed that the scatter plots obtained with pre-eigenanalysis 2D smoothing are more localized than that obtained using post-eigenanalysis 2D smoothing. Also, some outliers were incurred in this simulation example using post-eigenanalysis 2D smoothing. Note that the angle-delay parameters for the classical DS-CDMA communications systems are obtained blindly in the sense that we do not need to estimate the corresponding bit values in the joint estimation interval. In contrast, for the IS-95 uplink, we need use initialization algorithms or the decision directed mode in estimating Walsh symbols to determine which matched filter outputs would contain "RAKE fingers" for estimating the space-frequency correlation matrices.

7.2 Simulation Results for the IS-95 Uplink

The simulations presented here employ IS-95 uplink signal model parameters. The chip period is 0.8138 μs; the sampling rate was twice the chip rate; rectangular chip waveform was used. The number of half-chip spaced taps at each antenna used to encompass the delay spread was 16. The number of

Table 1: Signal and MUAI parameters

	Signal	MUAI1	MUAI2	MUAI3
SNR 1,2,3	x,x-1,x-3db	x+20,x+10, - db	x+4,x+6, - db	x,x-3, - db
Phase 1,2,3	$0^o, 45^o, 90^o$	$45^o, 50^o, -$	$-30^o, -35^o, -$	$180^o, 170^o, -$
AOA 1,2,3	$0^o, 7^o, 14^o$	$50^o, 55^o, -$	$-20^o, -23^o, -$	$-10^o, -7^o, -$
Delay 1,2,3 ($\times\frac{1}{2}T_c$)	0,3,8	$0, 3, -$	$0, 6, -$	$0, 10, -$

selected DFT samples was 9. $M = 8$ antennas were used. A three-ray multipath model was used for the desired user wherein the direct path arrived at an angle of 0^0 relative to broadside. The SNR's of the two specular multipaths were 1 and 3 dB below that the direct path and phase shifted by 90^0 and 45^0 at the array center, respectively. The relative delays of the specular multipaths for the desired source were $1\frac{1}{2}$ chip and four chips respectively; the elevation angles were 7^o and 14^o, respectively. To simulate multipath, each MUAI arrived via two paths having distinct arrival angles, time delays, and phase shifts. Both the desired source and the interferers were CDMA signals with different long PN codes and the same short I-Q PN codes. The generating polynomials for the long and short PN sequences are listed below [11].

$$
\begin{aligned}
g_L(x) = \quad & x^{42} + x^{35} + x^{33} + x^{31} + x^{27} + x^{26} + x^{25} + x^{22} + x^{21} + x^{19} \\
& + x^{18} + x^{17} + x^{16} + x^{10} + x^{7} + x^{6} + x^{5} + x^{3} + x^{2} + x^{1} + 1 \\
g_I(x) = \quad & x^{15} + x^{13} + x^{9} + x^{8} + x^{7} + x^{5} + 1 \\
g_Q(x) = \quad & x^{15} + x^{12} + x^{11} + x^{10} + x^{6} + x^{5} + x^{4} + x^{3} + 1
\end{aligned}
$$

We adjust the value of x to conduct the following simulations.

7.2.1 Results of the joint AOA and time delays estimates

Basic performance of the proposed joint estimation algorithms:

Example 1.:near-far problem scenario: The MUAI parameters in Table 1 are listed for the "near far" problem scenario. To simulate multipath, each MUAI arrived via two paths having distinct arrival angles, time delays, and phase shifts. Figure 5 displays the estimated AOA and delay "scatter plots" obtained from 1000 independent runs with the matrix pencil $\{\hat{\mathbf{K}}_{S+I+N}, \hat{\mathbf{K}}_{I+N}\}$ averaged over 10 Walsh symbol periods, and the input SNR x of the direct path signal equal to -20 db. The subarray size (m_1, m_2) was chosen to be $(6, 5)$. Similarly, it is observed that the scatter plots obtained with pre-eigenanalysis 2D smoothing are more localized than that obtained using post-eigenanalysis 2D smoothing. Also, some outliers were incurred in this simulation example using post-eigenanalysis 2D smoothing.

Example 2.equal input power scenario: Here we create a simulation scenario with equal input power for all the co-channel users. The signal of the desired user is the same as those of Example 1. The input SNR x of the direct path was equal to -20db. The other 40 users with different PN codes and single path were created with input SNR equal to -20db, and the AOAs were uniformly distributed within 120°. The other parameters are the same as those in Example 1. Figure 6 displays the estimated AOA and delay "scatter plots" obtained from 500 independent runs. This demonstrates that our estimation algorithms work well for both near-far problem and equal input power scenarios.

Performance comparison vs. CRB:

The bias of our joint estimation algorithms over the range of SNR's we simulated was found to be negligible. This facilitates the comparison with the Cramer Rao Bound (CRB). The simulation parameters are the same as those in Example 1. Due to better performance by using pre-eigenanalysis 2D smoothing estimation algorithm, Figure 7 only displays the comparison for this algorithm to the CRB while the number of Walsh symbols for averaging was varied from two to ten. The dash lines represent the CRB's for the estimates of each multipath component which are labelled with respect to the correct angle and delay parameters. Note that we did not generate interferers in this simulation example for the simplicity of comparison to the CRB by using the $\mathbf{K}_{I+N}$ expression in (38) with Gaussian noise only case.

7.2.2 Results of the application to the reduced dimension space-time 2D RAKE receiver

Basic performance of the reduced dimension space-time 2D RAKE receiver:

Figure 8 displays a typical result of the 64 normalized decision variables with the "correct" Walsh symbol index marked with 'x' for a single trial run for both the reduced dimension and the full dimension 2D RAKE receiver conducted at x = -21db in Table 1. The pre-eigenanalysis 2D smoothing algorithm was used in estimating $\{(\theta_i, \tau_i)\}, i = 1, 2, 3$. Once the first three Walsh symbols have been estimated (using either a training sequence or some blind initialization algorithm which was discussed in [9]), $\hat{\mathbf{K}}_{S+I+N}$ and $\hat{\mathbf{K}}_{I+N}$ were averaged over the three past Walsh symbol periods using only the one matched filter output per symbol corresponding to the estimated symbol, and the "largest" generalized eigenvector was applied to each of the 64 Walsh correlator outputs generated for estimating the next Walsh symbol as in a decision directed mode of operation. It shows that a significant increase in separation between the value of the true Walsh symbol decision variable and the other 63 decision variables can be achieved by using the knowledge of the angle-delay estimates to effect reduced dimension processing. Note that the size of the full dimension space-time correlation matrix is 128×128.

In contrast, the size of the reduced dimension correlation matrix is only 3×3. Figure 9 displays the mean (connected by the horizontal line) and standard deviation (64 vertical lines) of the respective magnitude of each of the 64 Walsh symbol decision variables for both the reduced dimension and the full dimension 2D RAKE receiver from 256 independent runs conducted at x = -21db. It is observed that the reduced dimension 2D RAKE receiver offers lower relative interference plus noise level and smaller standard deviation of the decision variables.

Convergence: full dimension space-time RAKE receiver v.s. reduced dimension space-time RAKE receiver:

Figure 10 displays the output SINR's of the full space-time processing and reduce dimension processing with AOA-delay estimates while the number of Walsh symbols for averaging $\hat{\mathbf{K}}_{S+I+N}$ and $\hat{\mathbf{K}}_{I+N}$ ($\{\hat{\mathbf{K}}^{st}_{S+I+N}, \hat{\mathbf{K}}^{st}_{I+N}\}$) was varied from two to ten, and the input SNR x in Talble 1 of the direct path signal equal to -20 db. The reduced dimension space-time 2D RAKE receiver is observed to yield a much larger output SINR when averaging over only a small number of symbol periods. This demonstrates faster convergence with reduced dimension processing. Therefore, reduced dimension processing is more feasible under the high variability of the mobile channel.

8 Conclusion

Simulation results show that our algorithms can accurately estimate the AOA and delay for each multipath under "near-far" conditions. The AOA information is useful for FDD downlink beamforming and source localization for emergency service. The pre-eigenanalysis 2D smoothing algorithm offers better performance than the post-eigenanalysis 2D smoothing algorithm. The paired AOA and delay information may be used to reduce the dimensionality of the space-time 2D RAKE receiver. Our simulation results show that better separation between the value of the true Walsh symbol decision variable and the other 63 decision variables may be achieved by using the knowledge of the paired angle-delay estimates, as opposed to that obtained with full dimension space-time processing. This better performance results from the faster convergence toward the optimal weight vector due to the reduced dimensionality under conditions of limited available symbols where channel characteristics remain approximately stationary.

References

[1] M. D. Zoltowski and Y-F Chen, "Joint angle and delay estimation for reduced dimension space-time RAKE receiver with application to IS-95 CDMA uplink," in *Proc. of 1998 IEEE Fifth*

International Symposium on Spread Spectrum Techniques and Applications (ISSSTA '98), Sep. 1998.

[2] M. D. Zoltowski, M. Haardt, and C. P. Mathews, "Close-form 2-D angle estimation with rectangular arrays in element space or beamspace via Unitary ESPRIT," *IEEE Trans. on Signal Processing*, vol. 44, Feb. 1996.

[3] Alle-Jan van der Veen, Michaela C Vanderveen, and Paulraj Arogyaswami, "Joint angle and delay estimation using shift-invariance techniques," *IEEE Trans. on Signal Processing*, vol. 46, pp. 405–418, Feb. 1998.

[4] G. G. Raleigh and T. Boros, "Joint space-time parameter estimation for wireless communication channels," *IEEE Trans. Signal Processing*, vol. 46, pp. 1333–1343, May 1998.

[5] B. Suard, A. Naguib, G. Xu, and T. Kailath, "Performance analysis of CDMA mobile communication systems using antenna arrays," in *Proc. ICASSP*, April 1993, vol. VI, pp. 153–156.

[6] E. G. Strom, S. Parkvall, S. L. Miller, and B. E. Ottersten, "DS-CDMA synchronization in time-varying fading channels," *IEEE Journal on Selected Areas in Communications*, vol. 14, no. 8, pp. 1636–1642, Oct. 1996.

[7] M. D. Zoltowski and J. Ramos, "Blind adaptive beamforming for CDMA based PCS/cellular," in *Conf. Rec. of 29th Asilomar IEEE Conf. on Signals,System, and Computers*, Nov. 1995, pp. 378–382.

[8] M. D. Zoltowski, Y.-F. Chen, and J. Ramos, "Blind 2D RAKE receivers based on space-time adaptive MVDR processing for the IS-95 CDMA system," in *Milcom '96*, Oct. 1996, pp. 618–622.

[9] Y-F Chen and M. D. Zoltowski, "Convergence analysis and tracking ability of reduced dimension blind space-time Rake receivers for DS-CDMA," in *VTC '98*, May 1998, pp. 2333–2337.

[10] P. Stoica and A. Nehorai, "Music, Maximum Likelihood, and Cramer-Rao Bound," *IEEE Trans. Acoustics, Speech, Signal Processing*, vol. 37, no. 5, pp. 720–741, May. 1989.

[11] TIA/EIA/IS-95 Interim Standard, *Mobile Station-Base Station Compatibility Standard for Dual Mode Wideband Spread Spectrum Cellular Systems*, Telecommunications Industry Association, 1993.

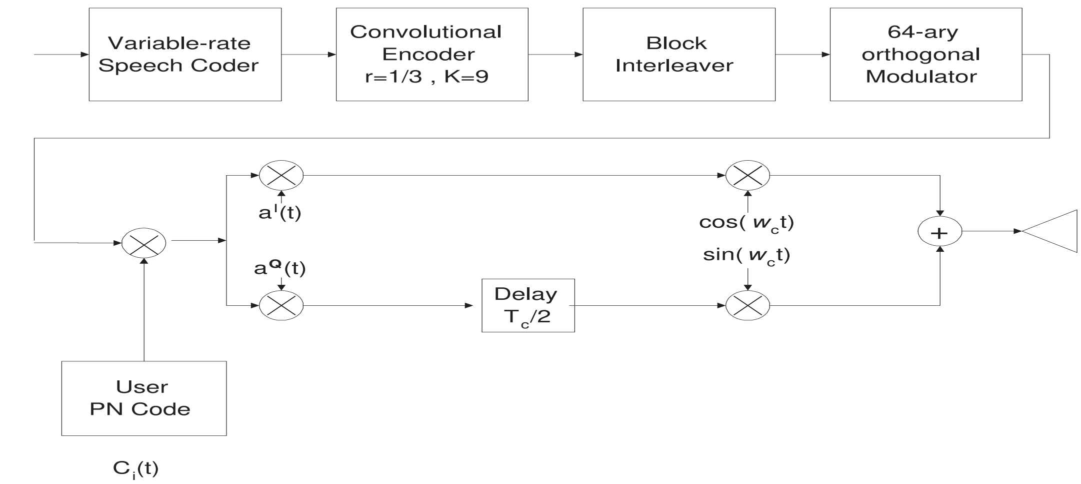

Figure 1: IS-95 uplink transmitter block diagram

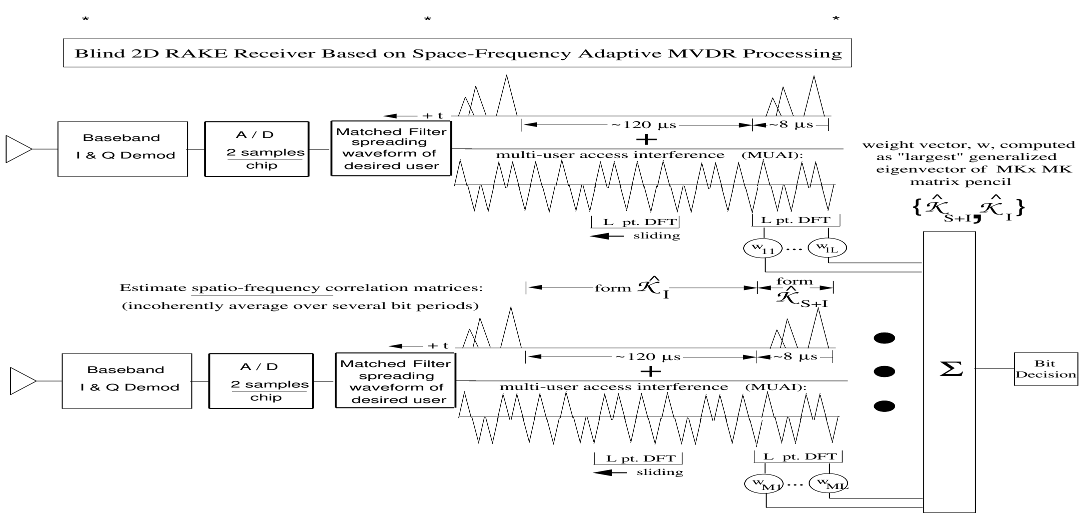

Figure 2: Diagram of the space-frequency 2D processing scheme

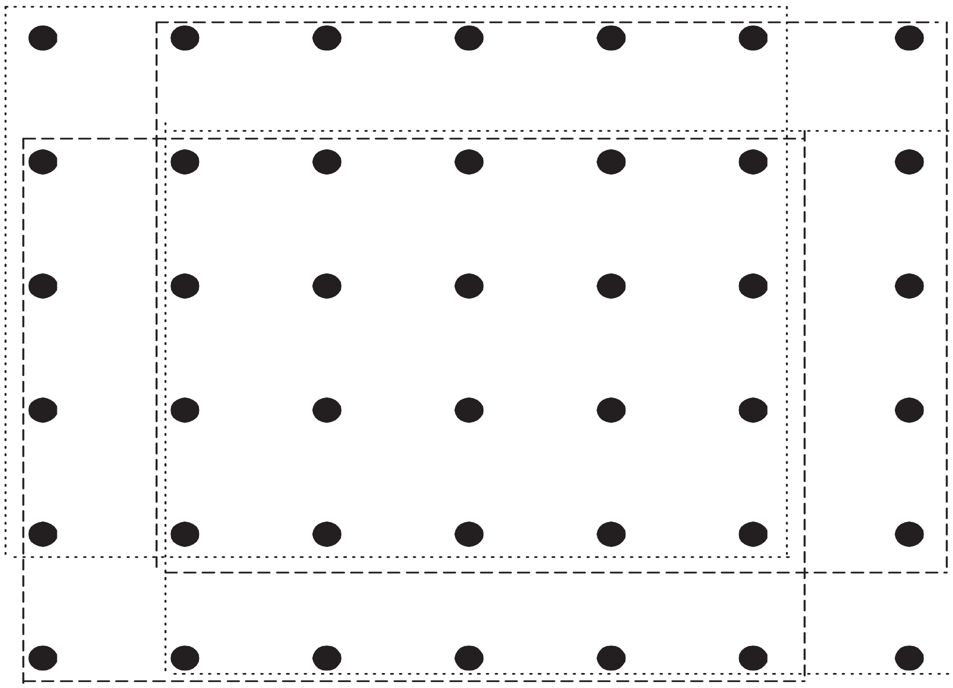

Figure 3: 2D smoothing : 2D subarray grouping with array size $(M \times L) = 6 \times 7$ and subarray size $(m_1 \times m_2) = 5 \times 6$

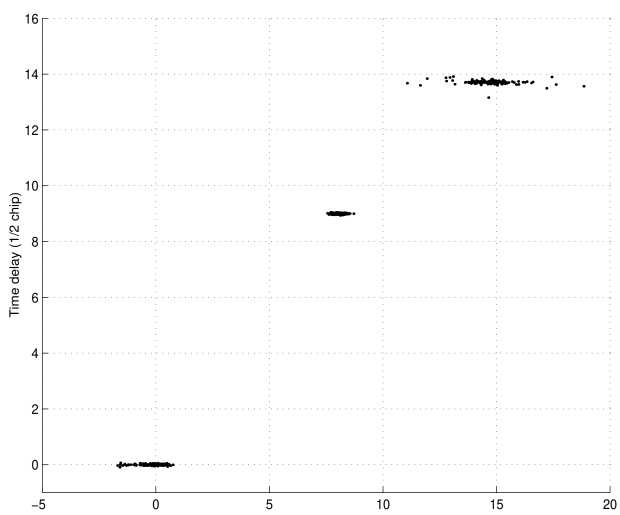

(a) Post-eigenanalysis 2D smoothing

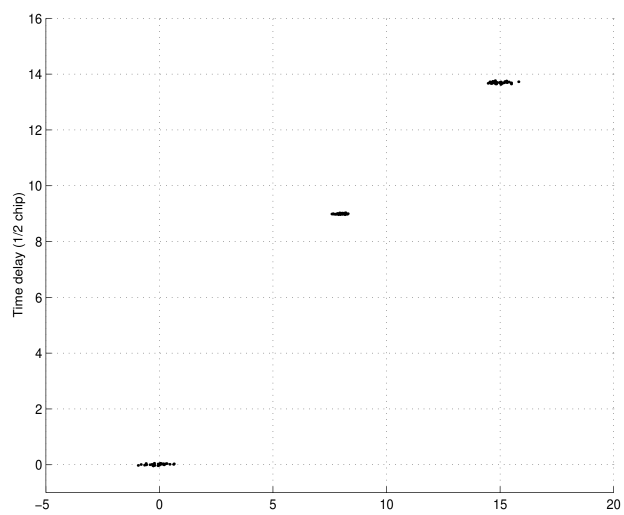

(b) Pre-eigenanalysis 2D smoothing

Figure 4: Scatter plots of the joint AOA-delay estimates for 256 trial runs (BPSK)

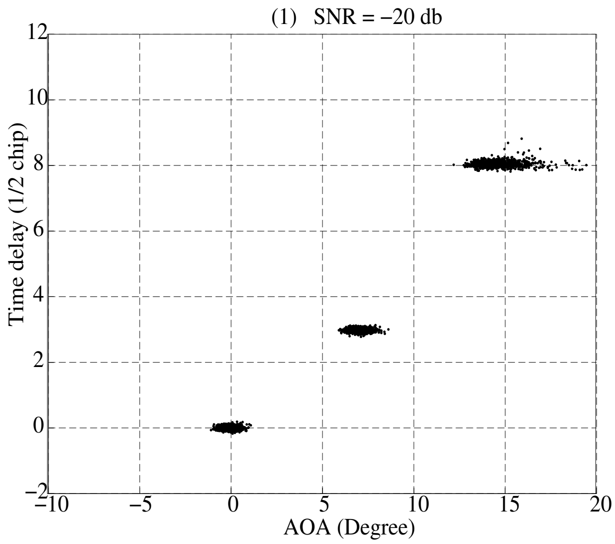

(a) Post-eigenanalysis 2D smoothing

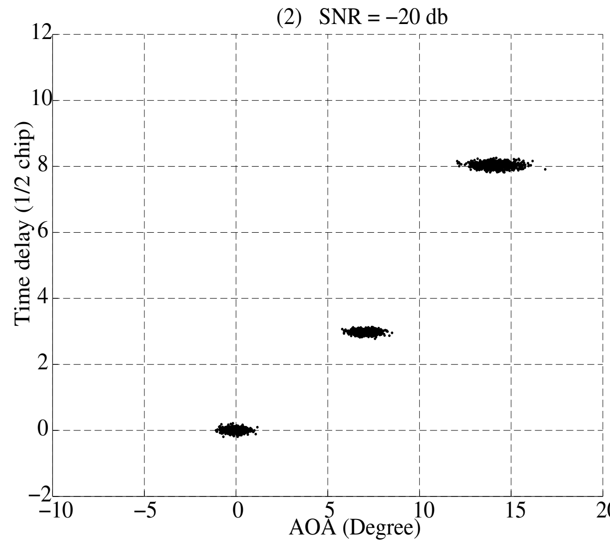

(b) Pre-eigenanalysis 2D smoothing

Figure 5: Scatter plots of the joint AOA-delay estimates under near-far problem scenario

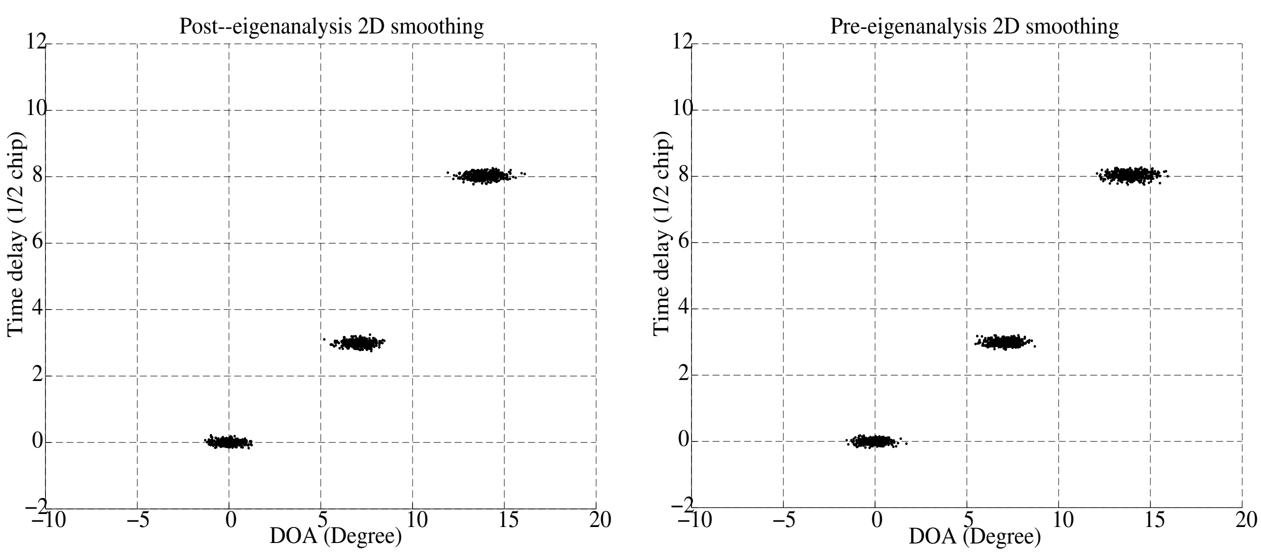

Figure 6: Scatter plots of the estimates under equal input power scenario

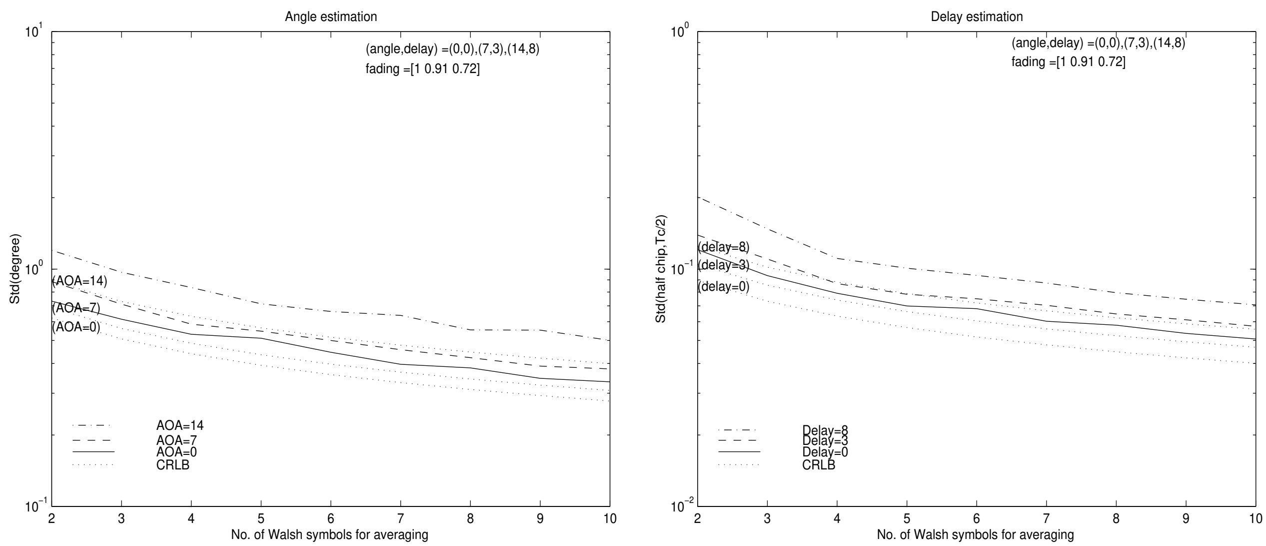

(a) Standard deviation of the AOA estimates (b) Standard deviation of the delay estimates

Figure 7: Performance comparison of the estimates (pre-eigenanalysis 2D smoothing) with the CRB

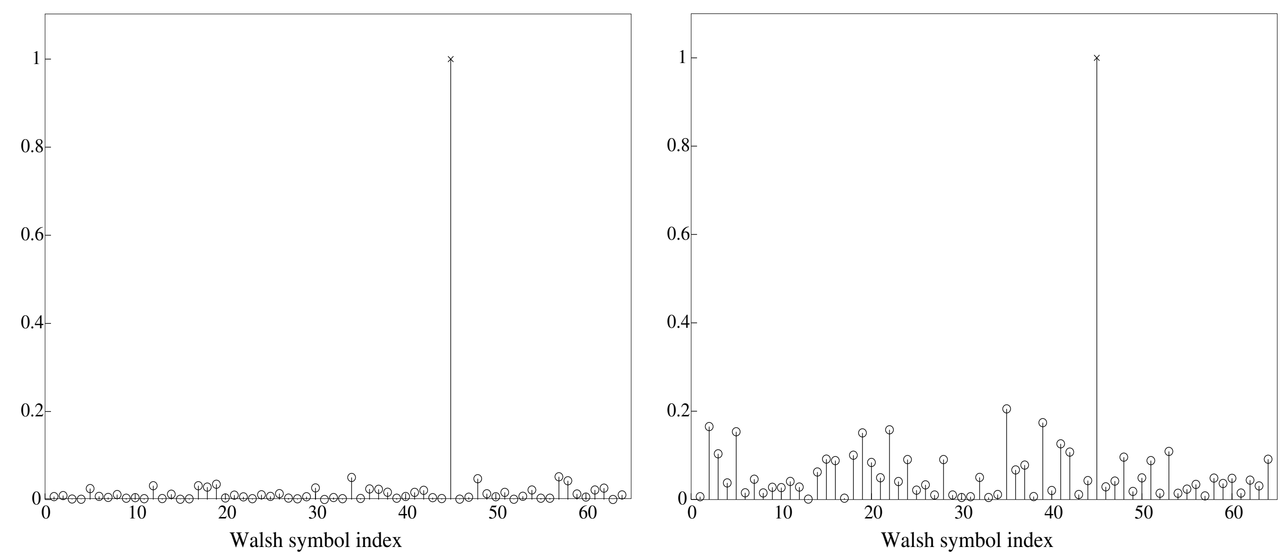

(a) Reduced dimension processing (b) Full dimension space-time processing

Figure 8: Typical result of the decision variables for a single trial run

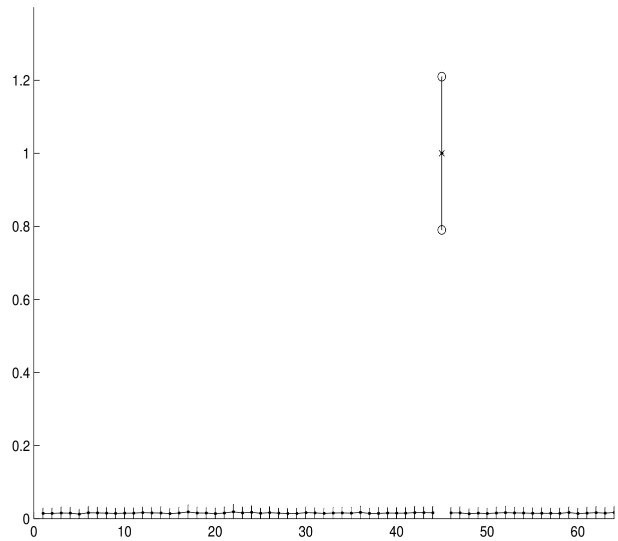

(a) Reduced dimension processing

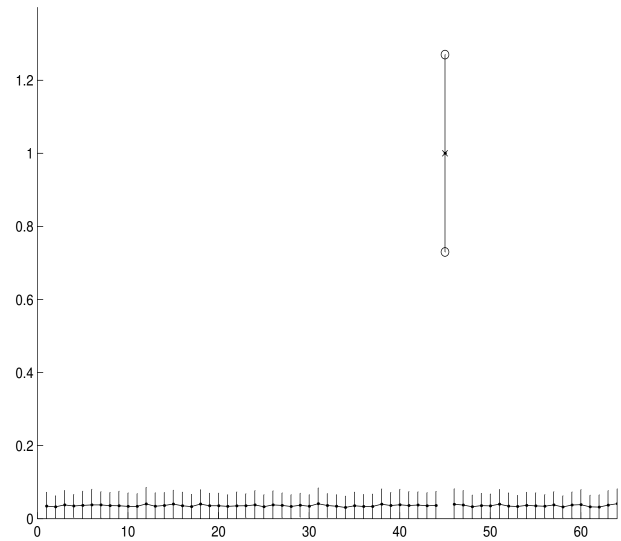

(b) Full dimension space-time processing

Figure 9: Mean and Standard deviation of the decision variables

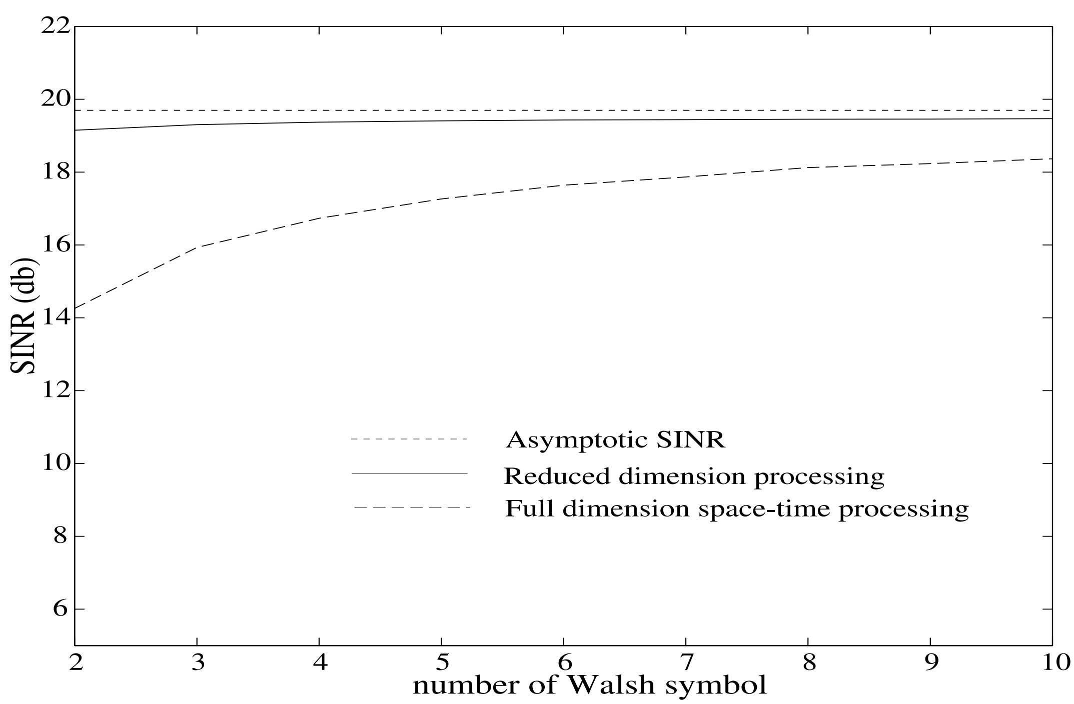

Figure 10: Convergence Comparison